

**ARTICLE**

Simulation of Offshore Wind Turbine Blade Docking Based on the Stewart Platform

Yi Zhang*, Jiamin Guo and Huanghua Peng

College of Ocean Science and Engineering, Shanghai Maritime University, Shanghai, 201306, China

*Corresponding Author: Yi Zhang. Email: Yizhang03166072@163.com

Received: 22 February 2023 Accepted: 10 April 2023 Published: 31 October 2023

ABSTRACT

The windy environment is the main cause affecting the efficiency of offshore wind turbine installation. In order to improve the stability and efficiency of single-blade installation of offshore wind turbines under high wind speed conditions, the Stewart platform is used as an auxiliary tool to help dock the wind turbine blade in this paper. In order to verify the effectiveness of the Stewart platform for blade docking, a blade docking simulation system consisting of the Stewart platform, wind turbine blade, and wind load calculation module was built based on Simulink/Simscape Multibody. At the same time, the PID algorithm is used to control the Stewart platform so that the blade can effectively track the desired trajectory during the docking process to ensure the successful docking of the blade. Through the simulation of the docking process for blades with a length of 61.5 meters, this paper successfully demonstrates a docking system that might facilitate future docking processes. It also shows that the Stewart platform can effectively reduce the vibration and the movement range of the blade root and improve the stability and efficiency of blade docking.

KEYWORDS

Offshore wind turbine; Stewart platform; blade docking; PID; Simscape Multibody

1 Introduction

In order to reduce carbon emissions, clean energy, including wind energy, has attracted wide attention. At present, the development of onshore wind power in China has become saturated. Offshore wind power has become a major development direction. This is because offshore wind power has significant advantages, such as not occupying arable land resources, stable wind power supply, and abundant wind energy resources [1]. Meanwhile, offshore wind power continues to develop from just off the coast to the far-reaching sea. However, the harsh marine environment makes the cost of blade installation account for 15%~20% of the total construction cost [2], which seriously restricts the construction and development of offshore wind power. At present, the blade is installed through a number of different methods such as full rotor lifting, rabbit ear lifting, and single blade lifting, in which the single blade installation can greatly improve the transportation efficiency of the installation ship and reduce the requirements for lifting equipment, significantly reducing the total installation cost [3].

At present, single-blade installation is the most widely used method. Single-blade installation first involves installing the nacelle and hub in place, then lifting the blades from the deck of the installation



ship to the docking height, and next positioning the blade root close to the hub by crane. After careful adjustment, the blade root bolts are placed into the hub bolt hole for fixing. The above process is only controlled by two wind ropes to help reduce blade oscillation, which is often insufficient for stable lifting and accurate docking of the blades, resulting in a slow installation process and damage to the blade and increasing the total cost of construction [4]. With the ongoing trend of installing larger and larger blades, installation difficulty will also increase significantly.

In order to cope with the above engineering problems, the researchers carried out research on blade wind load calculation, blade motion control, and construction equipment to improve the installation stability. Kuijken [5] established a multi-body dynamic model including blades, wind ropes, and yoke and analyzed the dynamic characteristics of blades under different wind conditions. Zhao et al. [6] developed a simulation tool to analyze the motion of the blade. In order to reduce the oscillation problem caused by wind load during the blade lifting process, Ren et al. [7] established a three-degree-of-freedom hoisting model, which combined the Kalman Filter and PID to control the sling and wind rope, effectively reducing the blade vibration under a high wind load and improving blade installation efficiency. At the same time, he used a motion estimation algorithm to predict the motion of the hub, thereby reducing the relative motion of the blade root to the hub [8]. Guo et al. [9] adopted the unscented Kalman Filter to reduce the noise in the lifting process of a single blade, further improving the stability of the blade in the lifting process. However, the above research only theoretically analyzed the blade movement under the control of wind rope without considering the problem of implementation, so it has low feasibility.

A numerical study [10] showed that the hub motion caused by wind and waves seriously affects the safety of blade docking. Verma et al. [11–13] analyzed the blade root damage caused by hub motion. At the same time, Verma et al. [14] and Jiang [15] adopted passively tuned mass dampers to reduce hub oscillation and hub impact on the blade to improve docking safety. In addition, some auxiliary lifting equipment has been successively developed and utilized to improve installation efficiency [16]. For example, the Blade Dragon [17] is a lifting yoke that can grip a blade and install it at different inclined angles; The Boom Lock [18] is an intelligence system that significantly reduces the blade motion. Although the above methods and equipment reduce the relative motion amplitude between the blade and the hub, they cannot control the movement of the blade root and cannot realize the rapid and stable alignment between the blade and the hub. Therefore, this paper will propose a new device to solve the above problems.

The Stewart platform, which has been widely used in spacecraft docking, ocean wave motion compensation, aircraft simulation, and other real-world scenarios, has the advantages of high structural stiffness, a strong bearing capacity, and limited motion error [19]. It can realize 6-DOF motion with high load and high precision. In the case of blade docking problems with high wind-induced loads and high alignment accuracy, the Stewart platform has the potential to play a significant role in improving docking stability, controlling the docking position, and reducing blade collision. The Stewart platform was developed based on the research of Stewart [20] and Gough et al. [21]. After years of development, the Stewart platform has been used in many engineering applications. For example, Ampelmann Company in the Netherlands used the Stewart platform for the development of offshore personnel transfer equipment [22]. FANUC, a Japanese company, designed the Stewart platform as an industrial robot for assembly and welding [23]. Many Chinese scholars [24–27] have researched parallel robots based on practical projects, and their achievements have promoted the application of parallel robots in many fields of engineering [28].

In this paper, the Stewart platform is used as an auxiliary tool for wind turbine blade docking. The ability to control the Stewart platform is used to reduce the blade root oscillation amplitude, improve docking stability under high wind speed conditions, and reduce the probability of collision between blades and hubs during the docking process. First, Simscape Multibody was used to conduct physical modeling for the Stewart platform and blade hoisting module, and the wind load calculation module was introduced [29]. Then, in a Simulink environment, the Stewart platform’s docking control capabilities were simulated for blades under high wind speeds. Finally, the simulation results were compared and analyzed.

2 The Stewart Platform

In order to adapt to the blade docking operations of offshore wind turbines, the Stewart platform structure had to first be improved. As shown in Fig. 1, based on keeping the structural characteristics of the Stewart platform unchanged, the dynamic and static platforms are changed into multi-segment assembled rings (two parts, C1 and C2, in Fig. 1). C1 and C2 are connected by a hinge and the connecting device. The Stewart platform can be disconnected at the “connecting device” and disengaged after the blade docking is complete. The improved dynamic and static platform is still connected by six arms, which are composed of prismatic joints, upper and lower rods, and universal joints [30]. The position of the dynamic platform is described by the fixed coordinate system $A - xyz$ and the moving coordinate system $B - x'y'z'$, and its attitude is described by the rotation matrix formed by the Euler Angle of RPY.

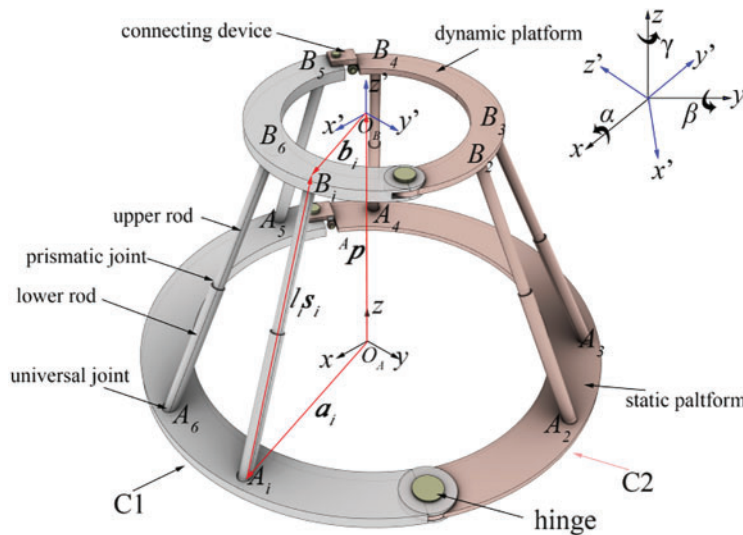


Figure 1: Coordinate system and computational model of the Stewart platform

In Fig. 1, the origin of coordinate systems A and B are located at the geometric centers of the static and dynamic platforms, O_A and O_B , respectively. The position vector of point P on the dynamic platform is represented by ${}^A\mathbf{P}$ in coordinate system A [31]:

$${}^A\mathbf{P} = [p_x \quad p_y \quad p_z]^T \tag{1}$$

The attitude of any point on the dynamic platform is the same as the attitude of frame B in frame A , which can be represented by the rotation matrix ${}^A\mathbf{R}_B$:

$${}^A\mathbf{R}_B(\alpha, \beta, \gamma) = \mathbf{R}_z(\gamma) \mathbf{R}_y(\beta) \mathbf{R}_x(\alpha) = \begin{bmatrix} c\beta c\gamma & s\alpha s\beta c\gamma - c\alpha s\gamma & c\alpha s\beta c\gamma + s\alpha s\gamma \\ c\beta s\gamma & s\alpha s\beta s\gamma + c\alpha c\gamma & c\alpha s\beta s\gamma - s\alpha c\gamma \\ -s\beta & s\alpha c\beta & c\alpha c\beta \end{bmatrix} \quad (2)$$

where: c represents \cos , s represents \sin ; $\mathbf{R}_x(\alpha)$, $\mathbf{R}_y(\beta)$, and $\mathbf{R}_z(\gamma)$ respectively represent the rotation matrix formed when the coordinate system A rotates α , β , and γ Angle (pitch Angle, roll Angle, and yaw Angle) about the x , y , and z axes of coordinate system A .

Suppose that the length matrix \mathbf{L} of the six arms is as follows:

$$\mathbf{L} = [l_1 \quad l_2 \quad l_3 \quad l_4 \quad l_5 \quad l_6]^T \quad (3)$$

When position ${}^A\mathbf{P}$ and attitude ${}^A\mathbf{R}_B$ of point O_B are known, the inverse kinematics analysis of the Stewart platform is carried out to find the value of matrix \mathbf{L} .

As shown in Fig. 1, the connection points between the i arm and the static and dynamic platforms are A_i and B_i , respectively, and the equation is as follows [32]:

$$l_i {}^A\mathbf{s}_i = {}^A\mathbf{P} + {}^A\mathbf{b}_i - {}^A\alpha_i = {}^A\mathbf{P} + {}^A\mathbf{R}_B {}^B\mathbf{b}_i - {}^A\mathbf{a}_i, \quad i = 1, 2 \dots 6 \quad (4)$$

where: \mathbf{a}_i is the vector $\overrightarrow{O_A A_i}$ in coordinate system A , \mathbf{b}_i is the vector $\overrightarrow{O_B B_i}$ in coordinate system B , ${}^A\mathbf{s}_i$ is the unit vector of the i arm in coordinate system A , and l_i is the length of the i arm, which can be calculated by the following Eq. (5).

$$l_i = \left[{}^A\mathbf{P}^T {}^A\mathbf{P} + {}^B\mathbf{b}_i^T {}^B\mathbf{b}_i + {}^A\mathbf{a}_i^T {}^A\mathbf{a}_i - 2 {}^A\mathbf{P}^T {}^A\mathbf{a}_i + 2 {}^A\mathbf{P}^T [{}^A\mathbf{R}_B {}^B\mathbf{b}_i] - 2 [{}^A\mathbf{R}_B {}^B\mathbf{b}_i]^T {}^A\mathbf{a}_i \right]^{1/2}, \quad i = 1, 2 \dots 6 \quad (5)$$

3 The PID Control Algorithm

In order to reduce the oscillation in the blade docking process, the dynamic platform was connected to the blade root. By controlling the position and attitude of the dynamic platform, the blade root was pulled to move in accordance with the desired trajectory of the platform to improve docking efficiency. This paper only considers the traction effect of the Stewart platform in the process of blade docking and ignores the possibility of collision between the blades and the hub. Therefore, the docking problem becomes fundamentally a problem with the motion control of the Stewart platform. The classical PID control algorithm [33] is adopted to control the driving force \mathbf{u} of the arm based on the length change of the arm so that the dynamic platform can achieve the desired position and attitude.

O_B is used as the reference point for motion control of the dynamic platform, and the pose λ of point O_B can be expressed in the coordinate system A as:

$$\lambda = [p_x \quad p_y \quad p_z \quad \alpha \quad \beta \quad \gamma]^T \quad (6)$$

Assuming that the desired trajectory of point O_B is λ_d , then the desired arm length \mathbf{L}_d is calculated using Eqs. (4) and (5), and the error between the desired and the actual value of the arm length is:

$$\mathbf{e} = \mathbf{L}_d - \mathbf{L} \quad (7)$$

The error value \mathbf{e} and the driving force \mathbf{u} of the arms are respectively used as the input and output parameters of the PID controller.

The control equation can be written as the following expression:

$$\mathbf{u}(t) = K_p \left[\mathbf{e}(t) + \frac{1}{T_i} \int_0^t \mathbf{e}(t) dt + T_d \frac{d\mathbf{e}(t)}{dt} \right], \quad K_i = K_p \frac{1}{T_i}, \quad K_d = K_p T_d \quad (8)$$

where: K_p , K_i , and K_d respectively represent the proportion, integral, and derivative coefficients; T_i is the integral time; and T_d is the derivative time.

The whole PID control process is shown in Fig. 2. The disturbing force F is the force transmitted by blade roots to the dynamic platform, and its magnitude is mainly caused by wind load. The specific calculation is determined by the wind load calculation module in the following section.

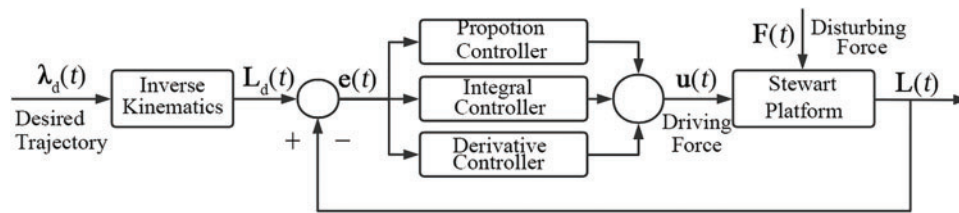


Figure 2: PID controller architecture

4 Blade Docking Simulation System

In this paper, Simulink/Simscape Multibody was used to establish the blade docking system, as shown in Fig. 3. The docking system mainly consists of three modules: Stewart platform, blades and wind load calculation. Among them, the functions of the Stewart platform module are Stewart platform building, inverse kinematics solving, and PID control. The functions of the blade module are setting up the blade model and the hoisting system, which includes the spreader, wind rope, and sling. The functions of the wind load calculation module are to simulate the wind field environment and calculate the wind load on the blades. In order to better simulate the variation of offshore wind speeds and test the effectiveness of the Stewart platform for blade motion control, the wind loads are generated through a superposition of average wind and turbulent wind. The whole simulation system ignores the influence of blade and Stewart platform deformation.

The docking analysis model built by the docking system is shown in Fig. 4. The whole docking model is located in the inertial coordinate system G . The spreader is fixed to the blade, and the four slings are connected with the four corner points of the spreader. The other end of the sling is connected to the same lifting point, which is connected directly to the apex of the crane. In order to ensure the stability of the docking process, the two corners of the spreader are each connected with a wind rope. The dynamic platform is connected to the blade root, and the center of the blade root coincides with the geometric center O_B of the dynamic platform, while the static platform remains stationary in the inertial frame G .

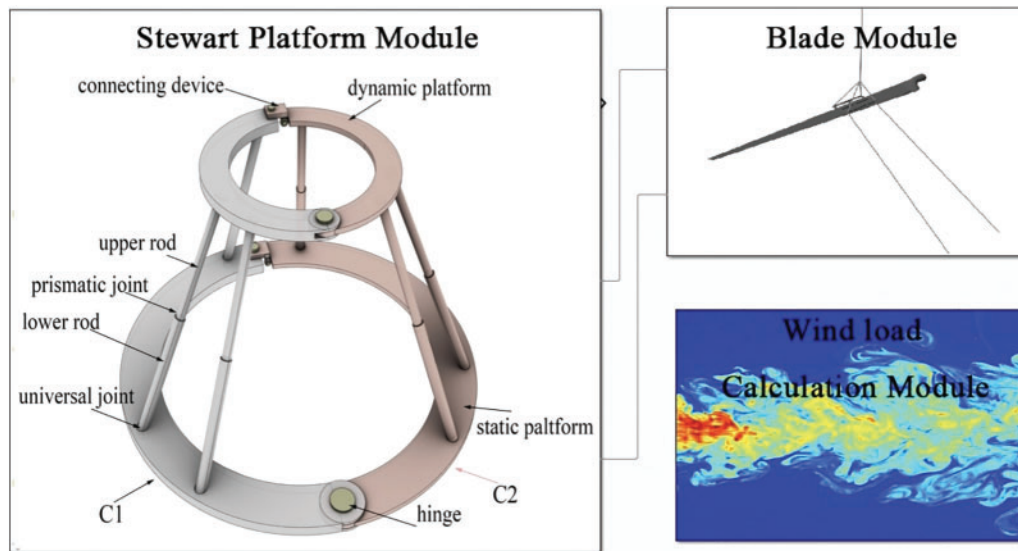


Figure 3: Composition of the docking system

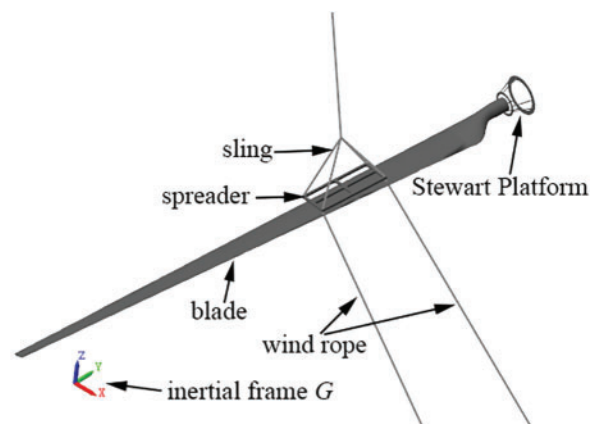


Figure 4: Docking system model

In the actual docking process, the blade root is maneuvered towards the hub by extending and shortening the arms of the Stewart platform. The docking process is completed when the guide bolt installed at the blade root enters the hole in the hub. After docking, the Stewart platform is removed.

5 Lifting and Alignment Simulation

In this paper, the docking system shown in Fig. 3 was used to conduct an alignment simulation for blades with a length of 61.5 m. The specific parameters of the docking system model shown in Fig. 4 are shown in Table 1. This paper analyzes how blades moving horizontally along the blade axis under a heavy wind load are docking. It is assumed that the initial position of the blade root center is located at the origin of the coordinate system G , so the trajectory of the blade root center in the coordinate system G is a straight line moving horizontally along the Y direction. Because the center of the blade

root coincides with the geometric center O_B of the dynamic platform, the desired trajectory $\lambda_d(t)$ of O_B in coordinate system A is:

$$\lambda_d(t) = [0 \quad 0 \quad p_z \quad 0 \quad 0 \quad 0]^T \tag{9}$$

Table 1: Parameters of docking system

Parameter	Value	Parameter	Value
Radius of dynamic platform/cm	38	q (amplitude)	20
Radius of static platform/cm	72	ω (angular frequency)	1
Length of upper rod/cm	40	ϕ (phase position)	$\Pi/2$
Length of lower rod/cm	56	h (offset)	10
K_p	50000	Blade length/m	61.5
K_i	400	Blade quality/t	17.74
K_d	400		

In order to ensure that the blade does not produce a large amount of shaking at the beginning and end of the docking process, the time-displacement curve of point O_B along the z-axis in coordinate system A is set as the following sine function:

$$p_z(t) = q \sin(\omega t + \phi) + h \tag{10}$$

where: t is time, q is amplitude, ω is angular frequency, ϕ is phase angle, and h is offset.

Traditional single-blade installation must be carried out under conditions where the average wind speed is less than 12 m/s. Therefore, three average wind speeds of 8, 10 and 12 m/s are selected in this paper in order to conduct accurate docking simulations. In order to understand the effectiveness of the Stewart platform in controlling the amplitude of blade root motion, simulations both with and without the Stewart platform were performed and compared in detail. The following expressions of orientation are all about the coordinate system G .

The wind speed simulation results at the blade root obtained by the wind load calculation module are shown in Fig. 5. Since wind loads are superimposed by combining average wind and turbulent wind, the wind speed at the blade root under the three different wind fields fluctuates greatly. When the average wind speed is 12 m/s, the fluctuation range is the largest, with the highest and lowest instantaneous wind speeds recorded as 16.8 and 7 m/s, respectively. The force and torque on the blade generated by the wind action are shown in Figs. 6 and 7.

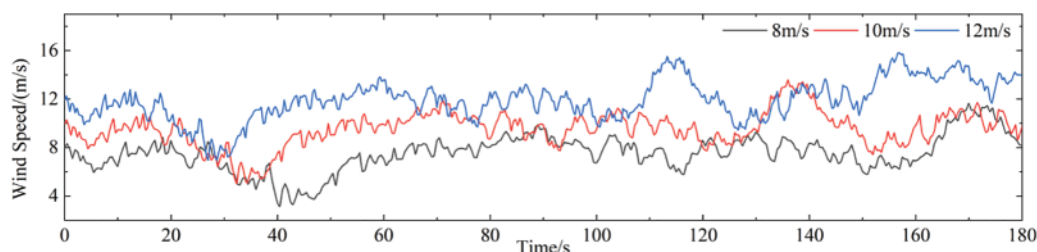


Figure 5: Wind speed change

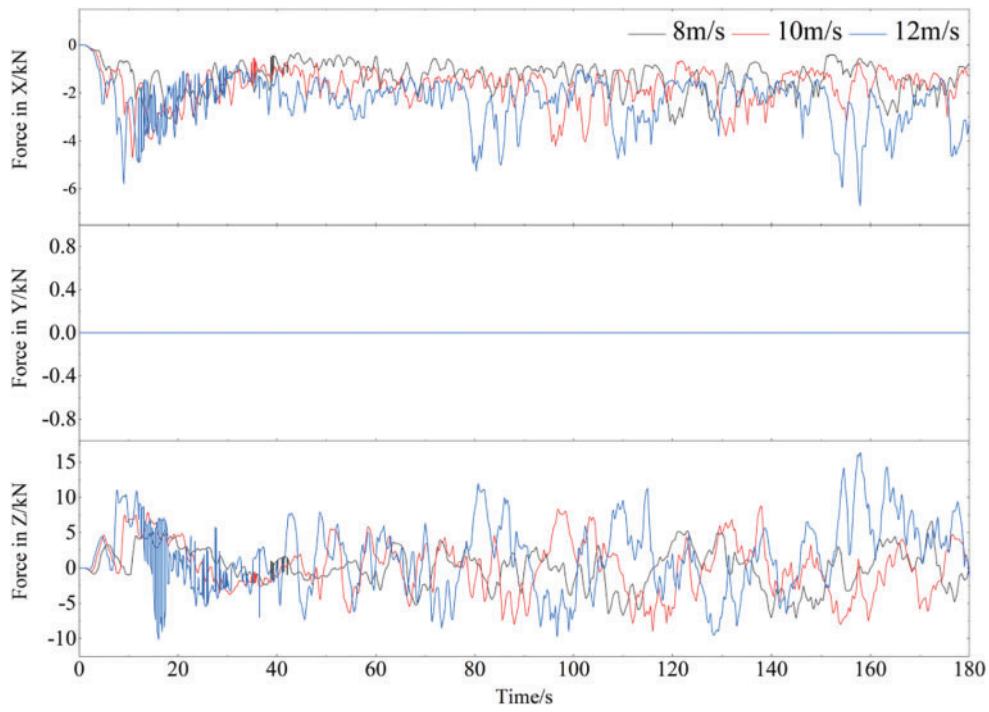


Figure 6: Wind-induced force of the blade

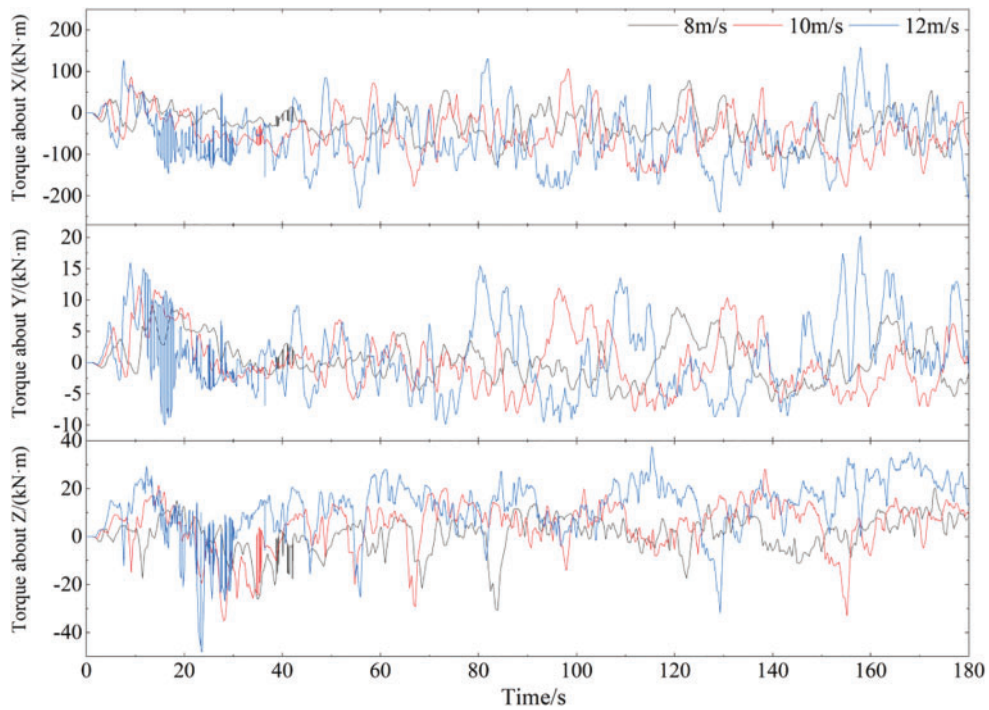


Figure 7: Wind-induced torque of the blade

As shown in Fig. 6, the maximum force is exerted in the Z direction, which is mainly caused by the aerodynamic characteristics of the blade. There is almost no force in the Y direction. Therefore, when setting the wind field, it can be assumed that the wind speed in the Y direction is functionally 0. Wind speed is only a variable on the XZ plane. In the X and Z directions, an increase in average wind speed leads to a corresponding increase in force on the blade. When the average wind speed is 12 m/s, the maximum force in the X direction is -6.7 kN. The maximum force in the Z direction is 16.4 kN, which varies from -10.1 to 16.4 kN.

As shown in Fig. 7, the variation in amplitude of torque increases with an increase in average wind speed. When the average wind speed is 12 m/s, the torque around the X-axis sees the highest variation, with a range of $-239.3\sim 157.9$ ($\text{kN} \cdot \text{m}$). The Y-axis torque ranges from $-9.9\sim 20.2$ ($\text{kN} \cdot \text{m}$), and the Z-axis torque ranges from $-48.1\sim 37.4$ ($\text{kN} \cdot \text{m}$).

The blade root center approaches the hub along the expected trajectory of Eq. (9), and its displacement changes in the Y, X, and Z directions are shown in Figs. 8–10.

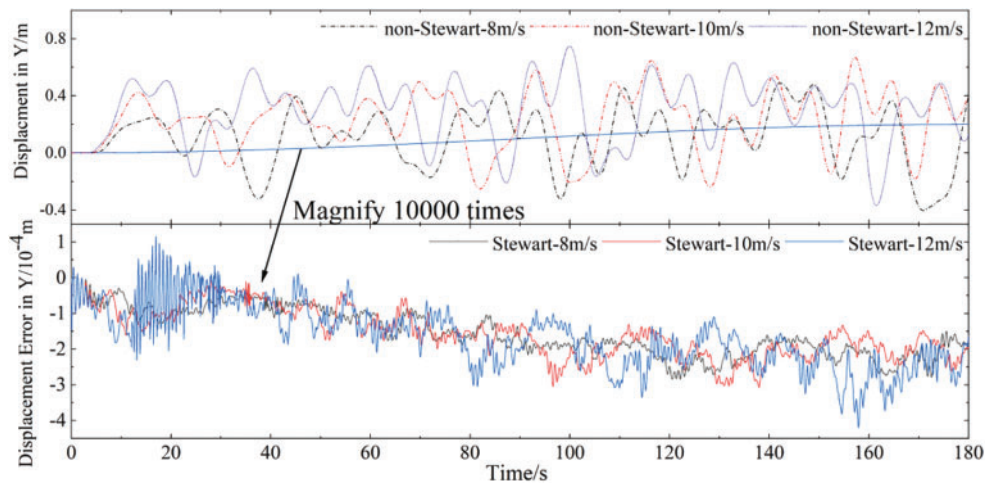


Figure 8: Displacement and displacement error of blade root in Y direction

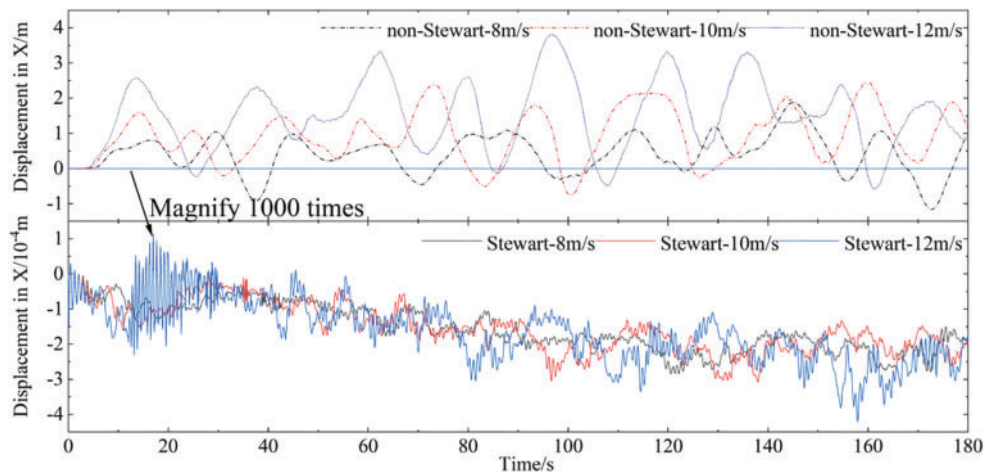


Figure 9: Displacement of blade root in X direction

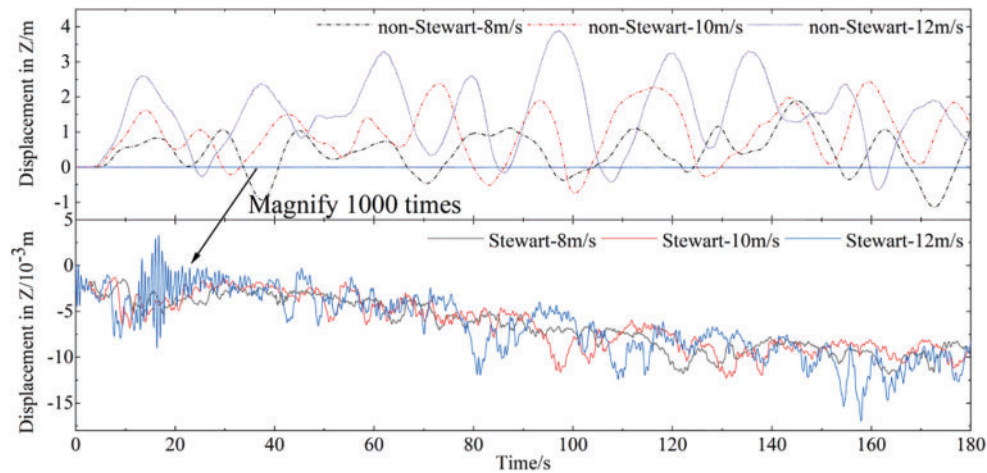


Figure 10: Displacement of the blade root in Z direction

As shown in Fig. 8, under the traction of the dynamic platform, the blade root moves from 0 to 0.2 m in the Y direction, and the displacement error in the Y direction is of the order of magnitude 10^{-4} m. When there is no Stewart platform, the displacement range of the blade under wind load in the Y-axis direction is $-0.40\sim 0.74$ m. As shown in Figs. 9 and 10, when there is no Stewart platform, blade roots move substantially in both the X and Z directions. With an increase in the average wind speed, the motion amplitude of the blade root also increases gradually. When the average wind speed is 12 m/s, the motion range in the X direction is $-0.58\sim 3.82$ m, and the motion range in the Z direction is $-0.64\sim 3.88$ m. The amplitude of blade motion due to wind-induced load will influence blade alignment significantly. When the Stewart platform is present, the motion amplitude of the blade roots in the X and Z direction will obviously be reduced, and the motion ranges are $-0.4\sim 0.1$ and $-1.7\sim 0.3$ cm, respectively. Therefore, it can be said that the Stewart platform provides greater control accuracy for blade alignment along the predetermined direction.

The changes in the attitude angle (pitch angle, roll angle, and yaw angle) at the blade root are shown in Fig. 11.

As shown in Fig. 11, the attitude angle gradually increases during the docking process. The main reason for the increase in attitude angle is that the blade root gradually deviates from its initial position due to wind load. However, when it comes to the amplitude of the attitude angle, the amplitude variation of the pitch angle, roll angle, and yaw angle are 10^{-3} , 10^{-2} and 10^{-3} rad, respectively. The variation range is all less than 0.03 rad, which further indicates that the Stewart platform can better control the rotation of blades around each axis.

The arm force with the largest change among the six arms are shown in Fig. 12. An increase in average wind speed results in a corresponding increase in the range of variation of arm force. Under the three wind speeds, the arm force increases continuously to maintain the stability of the blade root when the blade root gradually deviates from the initial position under the influence of high wind load.

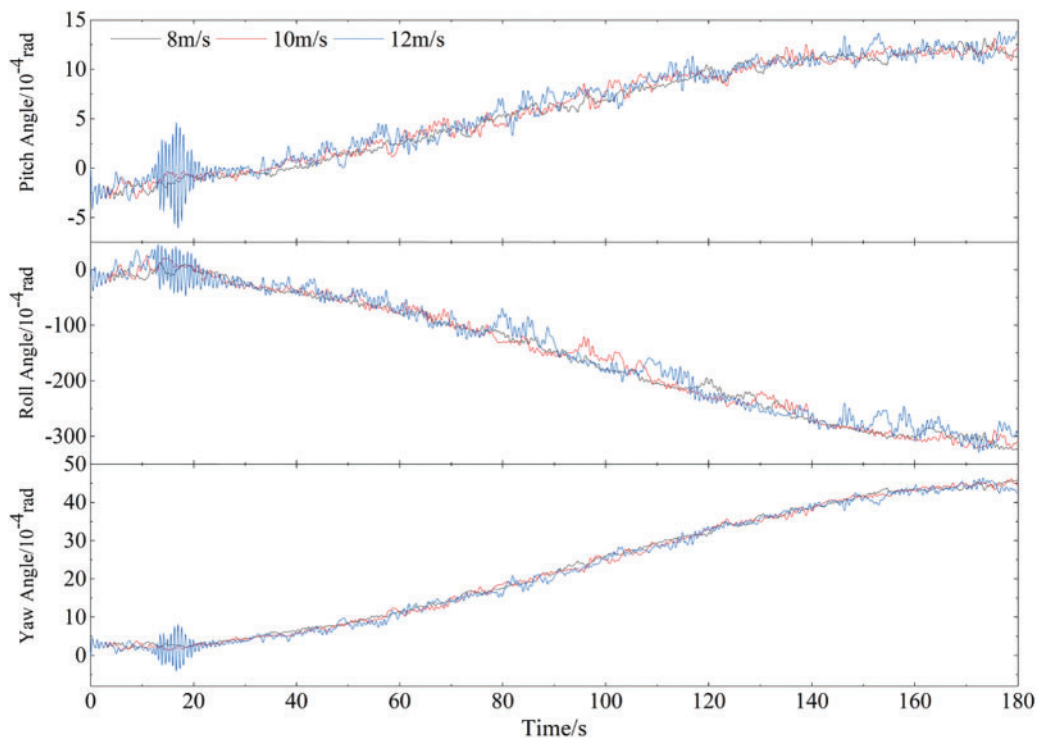


Figure 11: The changes in the attitude angle with Stewart platform

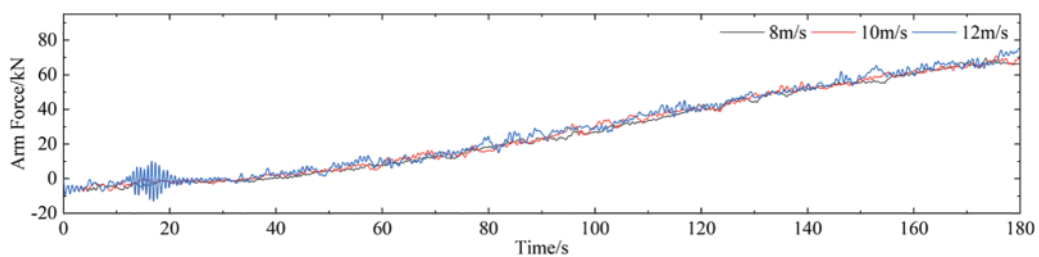


Figure 12: The changes of arm force

In summary, in the absence of the Stewart platform to control blade root movement and in the presence of strong winds, the maximum motion displacement of blades in each direction can reach several meters only through the passive connection of wind ropes. In this case, blade docking is completely impossible. When the Stewart platform is used to control the motion of the blade roots, the blade roots can move freely along the desired trajectory. In addition, the displacement error in all directions is less than 0.04 m and the displacement error in the Y direction is less than 4×10^{-4} m. The error rate of the change in attitude angle is less than 0.03 rad so that the blades can carry out the alignment work of blade roots under high wind speeds.

6 Conclusion

Based on the above research content, the main conclusions and contributions of this paper are as follows:

- (1) This paper analyzes the characteristics of the Stewart platform and the difficulties of docking offshore wind turbine blades and puts forward the research direction of applying the improved Stewart platform to the docking process of offshore wind turbine blades for the first time.
- (2) Based on Simulink/Simscape Multibody, this paper builds a blade docking simulation system, including the Stewart platform, blade, and wind load calculation module, which provides research tools for analyzing blade motion.
- (3) According to the simulation results, the Stewart platform docking system can effectively control blade movement following a desired trajectory. The motion displacement error in the Y-axis direction is less than 4×10^{-4} m, the motion error in the X and Z directions is less than 0.04 m, and the attitude angle error is under 0.03 rad. The Stewart platform greatly reduces the amplitude of blade root motion in all directions, enabling blade docking at high wind speeds.

This paper provides a theoretical basis for the application of the Stewart platform to the blade docking process, which will greatly improve the installation efficiency and safety of blades, reduce installation costs, and promote the development of offshore wind power.

Acknowledgement: No.

Funding Statement: The authors received no specific funding for this study.

Author Contributions: The authors confirm contribution to the paper as follows: study conception and design: Zhang Yi, Guo Jiamin; data collection: Zhang Yi; simulation model building: Zhang Yi; analysis and interpretation of results: Zhang Yi, Guo Jiamin, Peng huanghua; draft manuscript preparation: Zhang Yi, Guo Jiamin, Peng Huanghua. All authors reviewed the results and approved the final version of the manuscript.

Availability of Data and Materials: No.

Conflicts of Interest: The authors declare that they have no conflicts of interest to report regarding the present study.

References

1. Hu, W. S., Yang, X. G., Li, G. D., Guo, X. Y., Li, X. W. (2020). Analysis and suggestion of offshore wind power development of China. *Electric Power Technology and Environmental Protection*, 36(5), 31–36.
2. Shi, Z. Y. (2020). “Fourteen fifth plan” several considerations on offshore wind power development of China. *China Power Enterprise Management*, 41(13), 40–42.
3. Jiang, Z. Y. (2021). Installation of offshore wind turbines: A technical review. *Renewable and Sustainable Energy Reviews*, 139(44), 110576. <https://doi.org/10.1016/j.rser.2020.110576>
4. Zhou, G. X., Sun, H. F., Lei, C., Ge, C. (2022). Research on construction technology of 7.5 MW wind turbine blade lifting for offshore wind power. *Hydropower and New Energy*, 36(10), 24–27.
5. Kuijken, L. (2015). *Single blade installation for large wind turbines in extreme wind conditions: A quasi-steady aeroelastic study in high wind speeds under different inflow angles (Master Thesis)*. Delft University of Technology & Technical University of Denmark, Netherlands & Denmark.
6. Zhao, Y. N., Cheng, Z. S., Sandvik, P. C., Gao, Z., Moan, T. (2018). An integrated dynamic analysis method for simulating installation of single blades for wind turbines. *Ocean Engineering*, 152, 72–88.
7. Ren, Z. R., Jiang, Z. Y., Gao, Z., Skjetne, R. (2018). Active tugger line force control for single blade installation. *Wind Energy*, 21(12), 1344–1358.

8. Ren, Z. R., Skjetne, R., Jiang, Z. Y., Verma, A. S. (2019). Integrated GNSS/IMU hub motion estimator for offshore wind turbine blade installation. *Mechanical Systems and Signal Processing*, 123, 222–243.
9. Guo, J. M., Xie, Y. Y., Zhao, Y., Hou, X. R., Song, L. (2022). Offshore wind turbine blade hoisting control based on the unscented Kalman Filter. *Journal of Shanghai Maritime University*, 43(2), 112–119.
10. Jiang, Z. Y., Gao, Z., Ren, Z. R., Li, Y., Duan, L. (2018). A parametric study on the final blade installation process for monopile wind turbines under rough environmental conditions. *Engineering Structures*, 172, 1042–1056.
11. Verma, A. S., Jiang, Z. Y., Ren, Z. R., Gao, Z., Vedvik, N. P. (2020). Effects of wind-wave misalignment on a wind turbine blade mating process: Impact velocities, blade root damages and structural safety assessment. *Journal of Marine Science and Application*, 19(2), 1–16.
12. Verma, A. S., Jiang, Z. Y., Vedvik, N. P., Gao, Z., Ren, Z. R. (2019). Impact assessment of a wind turbine blade root during an offshore mating process. *Engineering Structures*, 180, 205–222.
13. Verma, A. S., Vedvik, N. P., Haselbach, P. U., Gao, Z., Jiang, Z. Y. (2018). Comparison of numerical modelling techniques for impact investigation on a wind turbine blade. *Composite Structures*, 209, 856–878.
14. Verma, A. S., Jiang, Z. Y., Gao, Z., Vedvik, N. P. (2020). Effects of a passive tuned mass damper on blade root impacts during the offshore mating process. *Marine Structures*, 72, 102778.
15. Jiang, Z. Y. (2018). The impact of a passive tuned mass damper on offshore single-blade installation. *Journal of Wind Engineering & Industrial Aerodynamics*, 176, 65–77.
16. Dong, F. (2021). Dongfang wind power's 10MW offshore wind turbine multi-functional spreader was born. *Power Equipment Management*, 8(2), 205.
17. Liftra (2023). LT975 blade dragon. <https://www.liftra.com/products/lt975-blade-dragon?time=2023-06-27T14:54:44Z>
18. High Wind, NV (2023). The boom in offshore. <http://www.high-wind.eu/wp-content/uploads/2015/09/high-windpdf-159955985281.pdf>
19. Liu, Y. H., An, D., Xv, Y., Shao, M., Liu, Z. P. et al. (2020). Kinematic analysis of space docking device of 6-UPS Stewart Parallel mechanism. *Machine Tool & Hydraulics*, 48(23), 150–154.
20. Stewart, D. (1966). A platform with six degrees of freedom: A new form of mechanical linkage which enables a platform to move simultaneously in all six degrees of freedom developed by Elliott-Automation. *Aircraft Engineering and Aerospace Technology*, 38(4), 30–35.
21. Gough, V. E., Whitehall, S. G. (1962). Universal tyre testing machine. *Proceedings of the 9th International Automobile Technical Congress*, pp. 117–137. London, UK.
22. Cerda Salzman, D. J. (2010). *Ampelmann: Development of the access system for offshore wind turbines (Master Thesis)*. Delft University of Technology, Netherlands.
23. FANUC (2018). F-200iB series. https://www.fanucamerica.com/docs/default-source/robotics-product-information-sheets/f-200ib-series_9.pdf?sfvrsn=f4faf90a_4
24. Huang, Z., Kong, L. F., Fang, Y. F. (1997). *Theory and control of parallel robot mechanism*. China: China Machine Press.
25. Huang, T., Wang, J. S., Whitehouse, D. J. (1999). Gough-Stewart platform kinematics design theory and method. *Scientia Sinica (Technologica)*, 1999(4), 310–320.
26. Liu, X. J. (2022). Thinking on the development of institutions and robotics. *Journal of Integration Technology*, 11(6), 1–4.
27. Liu, X. J. (2015). Innovation and application of robotic manufacturing equipment. *2015 China Automation Conference Abstract Collection*, pp. 47. Wuhan, China.
28. Ye, P. D., You, J. J., Qiu, X., Wang, L. K., Li, C. G. et al. (2020). Research status and development trend of kinematic performance of parallel robots. *Journal of Nanjing University of Aeronautics & Astronautics*, 52(3), 363–377.

29. Ren, Z. R., Jiang, Z. Y., Skjetne, R., Gao, Z. (2018). Development and application of a simulator for offshore wind turbine blades installation. *Ocean Engineering*, 166, 380–395.
30. Jiang, J. X. (2010). *Structure design and theoretical analysis of 6-PUS/UPS parallel robot (Master Thesis)*. Yanshan University, China.
31. Duan, Y. B., Liang, S. P., Zeng, D. X., Jiang, J. X., Zhao, Y. S. (2011). Kinematics and workspace analysis of a 6-PUS/UPU parallel robot. *Journal of Machine Design*, 28(3), 36–40.
32. Hamid, D. T. (2017). *Parallel robots: Mechanics and control*. China: China Machine Press.
33. Zhao, Y., Guo, J. M., Jiang, Z. Y., Chen, W. G., Zhou, G. G. (2022). Control method for determining feasible pre-stresses of cable-struts structure. *Thin-Walled Structures*, 174, 109159.